Stoichiometric Control of Lead Chalcogenide Nanocrystal Solids to Enhance Their Electronic and Optoelectronic Device Performance

Soong Ju Oh,[†] Nathaniel E. Berry,[†] Ji-Hyuk Choi,[†,⊥] E. Ashley Gaulding,[†] Taejong Paik,[§] Sung-Hoon Hong,[‡] Christopher B. Murray,[†,§] and Cherie R. Kagan[†,‡,§,*]

[†]Department of Materials Science and Engineering, [‡]Department of Electrical and Systems Engineering, and [§]Department of Chemistry, University of Pennsylvania, Philadelphia, Pennsylvania 19104, United States and [⊥]Complex Assemblies of Soft Matter, CNRS-Rhodia-UPenn UMI 3254, Bristol, Pennsylvania, 19007, United States

ABSTRACT We investigate the effects of stoichiometric imbalance on the electronic properties of lead chalcogenide nanocrystal films by introducing excess lead (Pb) or selenium (Se) through thermal evaporation. Hall-effect and capacitance—voltage measurements show that the carrier type, concentration, and Fermi level in nanocrystal solids may be precisely controlled through their stoichiometry. By manipulating only the stoichiometry of the nanocrystal solids, we engineer the characteristics of electronic and optoelectronic devices. Lead chalcogenide nanocrystal field-effect transistors (FETs) are fabricated at room temperature to form ambipolar, unipolar n-type, and unipolar p-type semiconducting channels as-prepared and with excess Pb and Se, respectively. Introducing excess Pb forms nanocrystal FETs with electron mobilities of 10 $cm^2/(V\ s)$, which is an order of magnitude higher than previously reported in lead chalcogenide nanocrystal devices. Adding excess Se to semiconductor nanocrystal solids in PbSe Schottky solar cells enhances the power conversion efficiency.

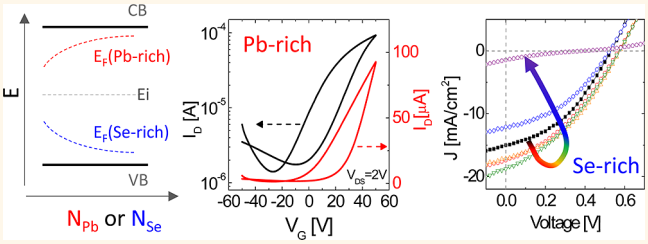

KEYWORDS: lead selenide · lead sulfide · nanocrystals · stoichiometry · field-effect transistor · photovoltaics

Nanocrystals (NCs) of the lead chalcogenides have been shown to be promising candidates for applications in electronics,[1,2] thermoelectrics,[3] and optoelectronics.[4−7] This family of materials has high carrier mobilities and low lattice thermal conductivities and is infrared absorbing. In the geometry of NCs, the electronic energy levels of this material may be tuned, and upon organization into NC solids, the transport of charge and heat can be tailored.[8] They also have the unique ability to switch the polarity of charge transport between ambipolar, n-type, and p-type, depending on the chemistry of surface-ligating compounds,[1] the presence of surface oxygen,[9] and the surrounding gas.[10] Stoichiometric imbalance is also known to change the polarity of transport in bulk and thin film lead chalcogenides of PbS, PbSe, and PbTe.[11] Pb-rich or X (X = S, Se, Te)-rich PbS,[12] PbSe,[13] and PbTe[14] were shown to become n-type or p-type, respectively. However, little is understood about the effects of stoichiometric imbalance on the electronic behavior of nanoscale lead chalcogenides and its influence on their devices. Stoichiometric imbalance may arise unintentionally during NC synthesis[15,16] or may be introduced intentionally during or after synthesis to manipulate the electronic properties of NC-based electronic materials.

Here, we directly study the effect of stoichiometric imbalance on the polarity of charge transport in PbS and PbSe NC thin film solids and utilize stoichiometric control to design electronic and optoelectronic devices. We tailor the stoichiometry of NC lead chalcogenide thin films by introducing excess Pb and Se through thermal evaporation and transform NC thin film device behavior from ambipolar to n-type and p-type, respectively [Figure 1A]. Using this method, we fabricate unipolar n-type and p-type lead chalcogenide NC field-effect transistors (FETs) with high performance at

* Address correspondence to kagan@seas.upenn.edu.

Received for review December 12, 2012 and accepted January 31, 2013.

Published online January 31, 2013
10.1021/nn3057356

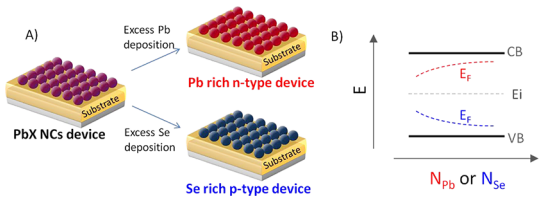

Figure 1. (A) Schematic of stoichiometric control of PbX NC thin films by Pb or Se deposition. (B) Fermi energy of PbX NCs as a function of the concentration of Pb (red) or Se (blue) atoms added to NC thin films.

room temperature. Quantitative analysis is performed by combining FET characteristics with Hall-effect measurements and capacitance−voltage ($C-V$) measurements. The carrier type, concentration, and Fermi level of as-synthesized and ligand-exchanged lead chalcogenide NC films show large variations that originate from unintentional doping during NC synthesis and device fabrication. We show that the carrier statistics can be precisely controlled by stoichiometric imbalance. As NC thin films become Pb-rich, the electron concentration increases and the Fermi level shifts toward the conduction band. As NC thin films become Se-rich, the hole concentration increases and the Fermi level drops toward the valence band [Figure 1B]. Finally, we utilize stoichiometric control to engineer carrier type and concentration to optimize PbSe NC Schottky solar cells to realize increased power conversion efficiency.

RESULTS AND DISCUSSION

PbX (X = S and Se) NCs capped with oleic acid are deposited by spin-coating to form NC thin film solids on substrates and in device geometries for structural, optical, electrical, and optoelectronic characterization. The long-chain oleic acid ligands capping the NCs, known to be insulating, are exchanged by treating the NC thin films with the compact ligands ammonium thiocyanate (NH_4SCN),[17,18] ethanedithiol (EDT),[9,19−22] hydrazine (N_2H_4),[1,22−24] and benzenedithiol (BDT)[25,26] [FTIR data in Supporting Information Figure S1] to decrease interparticle spacing and increase interparticle coupling. For example, in the case of SCN-exchanged PbSe NCs, small-angle X-ray scattering [Supporting Information Figure S2] shows reduced interparticle distance, and optical absorption data [Supporting Information Figure S3] show red shifts and broadening, signatures of enhanced electronic coupling.[18,27] Thermal evaporation of small amounts of Pb (range: 1 to 10 Å) and Se (range: 0.1 to 10 Å) are deposited to introduce a controlled stoichiometric imbalance in the NC thin films. No significant change in the absorption spectra of the NC thin films is observed upon Pb or Se deposition [Supporting Information Figure S3].

NC FETs are fabricated on heavily n-doped silicon wafers with 250 nm of thermally grown SiO_2, which

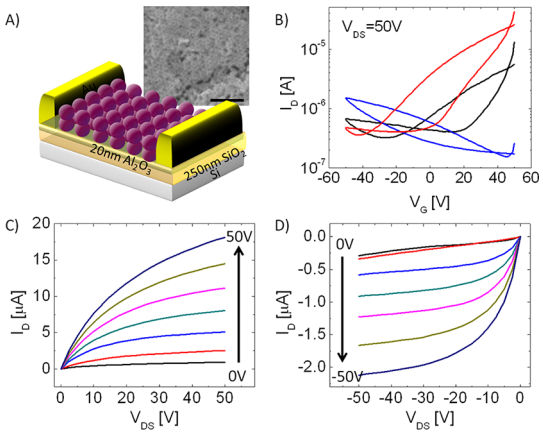

Figure 2. (A) Schematic of a PbX NC FET device and (inset) SEM image of a SCN-treated 6 nm PbSe NC thin film solid (scale bar: 100 nm); (B) transfer characteristics of (black) as-synthesized and exchanged (red) 1 Å excess Pb and (blue) 0.1 Å excess Se PbSe NC FETs and output characteristics of the (C) Pb-rich NC FETs with varying V_G from 0 V to 50 V and (D) Se-rich PbSe NC FETs with varying V_G from 0 V to −50 V.

serve as the back gate and part of the gate dielectric stack, respectively [Figure 2A]. Additionally, a 20 nm layer of Al_2O_3 is deposited by atomic layer deposition (ALD) on top of the SiO_2,[28] and the Al_2O_3 surface is derivatized with octadecylphosphonic acid (ODPA) to further reduce hysteresis and complete the dielectric stack.[29] Oleic acid capped PbX NCs are spin-coated onto the substrate and soaked in a compact ligand solution. The spin-coating and ligand exchange procedure are repeated twice to achieve a film thickness of ∼30 nm. The 40 nm Au source and drain top contacts separated by 50 to 150 μm are defined by thermal evaporation through a shadow mask.

Using this design, we fabricate as-synthesized, SCN-exchanged PbSe NC FETs that show ambipolar behavior [Figure 2B]. This is expected because PbSe has similar electron and hole mobilities,[12] PbX NCs are small band-gap materials providing a small barrier to both electron and hole injection, and the NCs are handled using air-free techniques, preventing oxygen exposure, which may cause significant p-doping.[10,28] We note that from sample to sample predominantly n- or p-type ambipolar behavior may be observed. This can be attributed to a combination of unintentional nonstoichiometry in NC composition, which is known to give rise to slightly Pb-rich PbX NCs[15,16,30] that favor predominantly n-type behavior, and unintentional surface oxygen p-type doping, which occurs even at the <0.1 ppm levels of oxygen in nitrogen-filled gloveboxes.[10,26,28,31] We denote this unintentional change in carrier concentration by Δn_{un}, and when it is on the order of the intrinsic carrier concentration, where n_e (electron concentration) is equal to n_h (hole concentration), the electron and hole currents and mobilities vary unexpectedly. As-prepared, SCN-exchanged PbSe NC FETs show an electron mobility of

0.02(±0.005) cm^2/(V s) in predominantly n-type ambipolar devices and a hole mobility of 0.01(±0.004) cm^2/(V s) in predominantly p-type ambipolar devices with $I_{ON}/I_{OFF} \approx 10^2$. The electron mobility in predominantly p-type devices and hole mobility in predominantly n-type devices are smaller than 10^{-4} cm^2/(V s).

While an as-prepared FET shows ambipolar characteristics, the transfer characteristics [Figure 2B] show that deposition of 1 Å of Pb makes the film n-type in all cases, suppressing the hole current and increasing the electron current and mobility. Similarly, the deposition of 0.2 Å of Se makes the film p-type, decreasing the electron current and enhancing the hole current and mobility. Figure 2(C and D) shows the output characteristics of n-type Pb-rich and p-type Se-rich PbSe NC FETs, respectively. We conducted control experiments in which 10 Å of Pb and 10 Å of Se were deposited between the source and drain electrodes in device structures without NCs and confirmed that these configurations are insulating, showing no current above the 5 pA noise level of the measurement.

Different thicknesses of Pb, ranging from 1 to 4 Å, and Se, ranging from 0.1 to 0.4 Å, were deposited on top of the PbSe NC FETs by thermal evaporation. As the amount of Pb (Se) is increased, the hole (electron) current decreases and electron (hole) current increases [Figure 3A, B]. In addition, the threshold voltage shifts to negative (positive) voltages, indicating a shift in the Fermi level toward the conduction band (valence band) and thus making the film more n-type (p-type) [Figure 1B].[32] While as-prepared devices show large variations in their electrical properties due to $\Delta n_{un} \approx n_e$ or n_h, in Pb- and Se-rich devices the mobility and current level can be precisely controlled by the amount of material deposition. This is because Δn_{st} (change of carrier concentration by stoichiometric control) is much larger than Δn_{un}, as will be discussed in the Hall and $C-V$ measurement sections.

In the range $V_G = -50$ to 50 V, as Pb or Se is deposited, I_{ON}/I_{OFF} first increases up to a maximum value. As more material is deposited, I_{ON}/I_{OFF} decreases, the current level increases, and the devices eventually become metallic, characteristic of a heavily doped, degenerate semiconductor. When 8 Å of Pb or 1 Å of Se is deposited, the films show semimetallic behavior. This trend, observed by introducing nonstoichiometry in NC thin films, generally agrees with bulk or thin film PbSe, where a large deviation from stoichiometric balance results in degenerate characteristics.[13]

High-performance semiconductor PbSe NC thin film FETs are fabricated entirely at room temperature with a linear electron mobility of 9.0(±2) cm^2/(V s) [Figure 3C] and a saturation electron mobility of 11(±2) cm^2/(V s) with I_{ON}/I_{OFF} of ~10^2, when 2 to 3 Å of Pb are deposited, which is the highest reported mobility among the lead chalcogenide NC FETs. It should be noted that our high mobilities are not the artificial results of hysteresis.

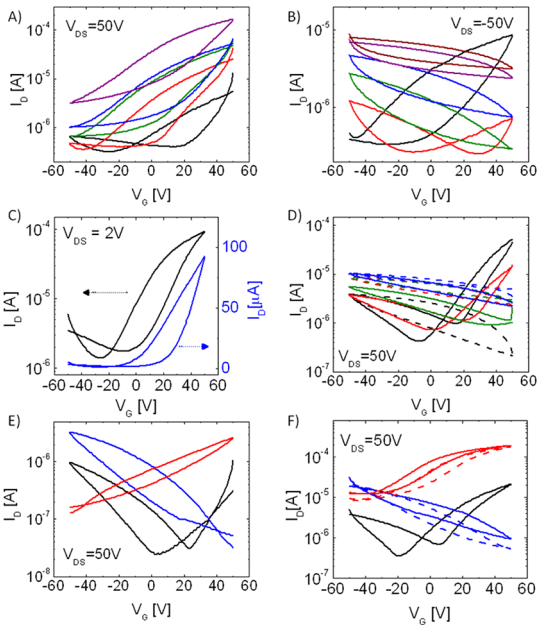

Figure 3. (A) Transfer characteristics of PbSe NC FETs in the saturation regime (black) before and after (red) 1 Å, (green) 2 Å, (blue) 3 Å, and (purple) 4 Å of Pb deposition. (B) Transfer characteristics of PbSe NC FET devices in the saturation regime (black) before and after (red) 0.1 Å, (green) 0.2 Å, (blue) 0.3 Å, (purple) 0.4 Å, and (brown) 0.5 Å of Se deposition. (C) Transfer characteristics of a PbSe NC FET in the linear regime after 3 Å of Pb deposition. (D) Transfer characteristics of PbSe NC FETs in the saturation regime with an NC channel thickness of (black) 35 nm, (red) 70 nm, (green) 105 nm, and (blue) 140 nm. Dashed line and solid line indicate before and after deposition of 1 Å of Pb, respectively. (E) Transfer characteristics in the saturation regime of SCN-treated PbS NC FETs (black) before and after (red) 2 Å excess Pb and (blue) 0.2 Å excess Se deposition. (F) Transfer characteristics in the saturation regime (black) before and after (red) 2 Å excess Pb and (blue) 0.2 Å excess Se PbSe NC FETs. Solid and dashed lines indicate before and after 12 h under vacuum of 10^{-7} Torr.

When FETs display large hysteresis, they show two different mobilities coming from two very distinct transconductances (dI_D/dV_G)[33] depending on the scan directions. One mobility will be unrealistically high, while the other will be very low, and neither has physical meaning when hysteresis is huge. Kang *et al.*[33] showed meaningful mobility could not be extracted at room temperature from PbSe NC FETs due to large hysteresis. However, our devices, as represented by the device characteristics in Figure 3C, show both a high linear mobility of 10 cm^2/(V s) in the reverse scan and a mobility of 5 cm^2/(V s) in the forward scan direction. Our hysteresis is lower in part because we employ ODPA self-assembled on Al_2O_3 in the gate dielectric stack to reduce the trap density at the NC−dielectric interface.[29] Additionally, the hysteresis (ΔV_T) in FETs with excess Pb is greatly reduced ($\Delta V_T = 25$ V) as excess Pb passivates surface trap states, in comparison to as-prepared NC FETs ($\Delta V_T = 60$ V). When 0.2 to 0.3 Å of Se are deposited, NC FETs show a linear hole mobility of 0.3(±0.05) cm^2/(V s) and a saturation hole mobility of

TABLE 1. Hall Measurement Data

	intrinsic	Pb 3 Å	Pb 10 Å	Se 3 Å	Se 10 Å
carrier type	holes or electrons[a]	electrons	electrons	holes	holes
Hall coefficient (cm^3/C)	69 ± 18	2.8 ± 0.3	0.52 ± 0.1	8.92 ± 0.7	2.8 ± 0.4
carrier concentration (cm^{-3})	$(9 \pm 6) \times 10^{16}$	$(2.2 \pm 0.3) \times 10^{18}$	$(1.2 \pm 0.2) \times 10^{19}$	$(7 \pm 1) \times 10^{17}$	$(2.2 \pm 0.2) \times 10^{18}$
Hall mobility ($cm^2/(V\ s)$)	0.28 ± 0.15	0.40 ± 0.05	0.44 ± 0.06	0.33 ± 0.08	0.34 ± 0.05

[a] Concentration type varies sample to sample, but predominantly shows the majority carriers to be holes.

$0.5(\pm 0.1)\ cm^2/(V\ s)$. The FETs have I_{ON}/I_{OFF} of 10^1 to 10^2 and slightly reduced hysteresis ($\Delta V_T = 55$ V). Depositing excess metal (Pb) consistently gives rise to higher current and higher mobility than the introduction of excess chalcogen (Se). Surface states within the band gap of nonstoichiometric PbSe NCs have been theoretically studied and are associated with dangling Se bonds above the valence band maximum and dangling Pb bonds below the conduction band minimum.[34] Further study is needed to investigate the energies and concentrations of electron and hole trap states introduced through nonstoichiometry that give rise to the difference in the observed carrier mobilities and current levels in devices.

We investigate the diffusion length of thermally evaporated Pb and Se atoms in the NC thin film by studying the polarity of charge transport in bottom contact PbSe NC FETs[35] with channel thicknesses ranging from 10 to 150 nm. The region of the NC thin film channel for which the conductance may be modulated by the gate voltage is the layer within the Debye screening length from the interface with the bottom gate dielectric layer. The Debye length (L_D) in the NC thin film can be calculated as

$$L_D = \left(\frac{\varepsilon_s \varepsilon_0 k_B T}{e^2 n}\right)^{0.5} \quad (1)$$

where ε_s is the effective dielectric constant of the NC thin film, ε_0 is the vacuum permittivity, k_B is the Boltzmann constant, e is the electric charge, and n is the carrier concentration. We found ε_s to be 24 for a film composed of 6 nm PbSe NCs (see Supporting Information). Given that L_D varies inversely with n [plot of L_D as a function of n in Supporting Information Figure S4], for as-prepared PbSe NC films we calculate $L_D \approx 20$ nm, which corresponds to around three layers of 6 nm NCs. Therefore, NCs in the film beyond the first 20 nm from the semiconductor−gate dielectric interface will contribute relatively little to the conductance modulation of the majority carrier in the device. As seen in Figure 3D, 1 Å of Pb can switch the FET polarity to n-type when the film is thinner than 105 nm, but it cannot change the device polarity when the film is thicker than 105 nm, indicating that 1 Å of Pb can diffuse up to at least ~60−80 nm. Similarly, 0.2 Å of Se can diffuse up to at least 50−70 nm [Supporting Information Figure S5]. This partial conduction-type change promises the fabrication of more complicated architectures such as p−n or p−i−n junctions by multiple deposition of Pb or Se at different thicknesses.

PbSe NC FETs treated with 1 M hydrazine [note: 1 M hydrazine treatment for 5 min is insufficient to achieve unipolar n-type behavior, and devices show predominantly n-type ambipolar behavior[6]], EDT, and BDT also show similar transformations when extra Pb or Se is deposited [Supporting Information Figure S6]. Regardless of the composition of the ligand, PbSe NC FETs display n-type behavior when Pb-rich and p-type behavior when Se-rich. We find that this method of achieving n-type and p-type films can be applied to other lead chalcogenides. Pb-rich PbS and Se-rich PbS NC FET transfer curves are shown in comparison to as-prepared devices in Figure 3E. It should be noted that PbS NC devices show a larger increase in hole current than PbSe NC FETs when the same amount of Se is deposited.

The stability and reversibility of the polarity of these NC films are studied under vacuum. The n-type Pb-rich stoichiometry proves stable, as FET characteristics are almost unchanged after 12 h under 10^{-7} Torr vacuum [Figure 3F]. This is in direct contrast to the hydrazine treatment, the only other reported method in the literature to our knowledge capable of making lead chalcogenide NC FETs unipolar n-type with mobility higher than $1\ cm^2/(V\ s)$. NC FETs treated with hydrazine are not stable under vacuum due to hydrazine desorption.[1] During the preparation of this paper, the Sargent group reported n-type lead chalcogenide NC thin films achieved through doping with iodine. While these NC thin films have not yet shown as high electron mobilities as ours, they provide another promising route to n-type NC thin film materials.[36−38] The p-type effect of Se-rich stoichiometry is similarly stable under vacuum [Figure 3F]. Vacuum-stable NC doping is technologically important, as vacuum deposition of metal contacts is commonly employed in the construction of NC solar cells, thermoelectrics, and FETs.

To obtain more quantitative data on carrier type and concentration, we conduct Hall measurements using 70 nm spin-coated PbSe NC thin films. Table 1 compares the carrier type, Hall coefficients, carrier concentrations, and Hall mobilities of PbSe NC thin films as-prepared and for different introduced excesses of Pb and Se. As-synthesized, SCN-exchanged PbSe NC thin films are primarily p-type with a majority carrier hole

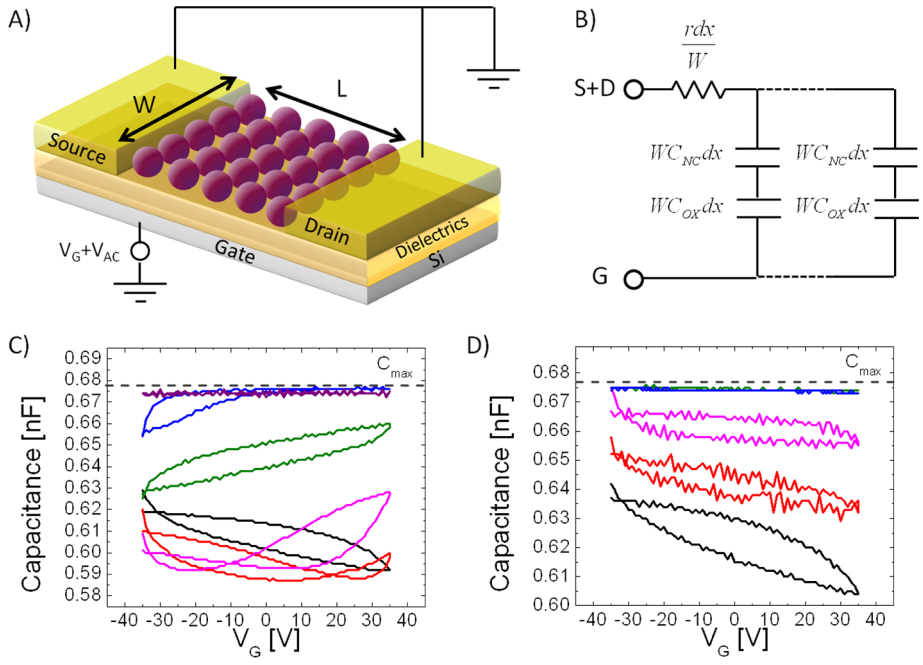

Figure 4. (A) Schematic of a metal−semiconductor (PbSe NC thin film)−insulator−metal (MSIM) structure for capacitance voltage (*C*−*V*) measurements; (B) equivalent circuit of the channel where *r* is the sheet resistance, *dx* is the elements of length in the channel, *W* is the channel width, C_{NC} is capacitance of the NC thin film, and C_{OX} is the capacitance of oxide in the channel; (C) *C*−*V* plot (black) before and after (red) 0.3 Å, (pink) 0.6 Å, (green) 0.9 Å, (blue) 1.2 Å, and (purple) 2 Å of Pb deposited; (D) *C*−*V* plot (black) before and after (red) 0.3 Å, (pink) 0.6 Å, (green) 0.9 Å, and (blue) 1.2 Å of Se deposited.

concentration of $(9 \pm 6) \times 10^{16}$ holes/cm^3, but films may also be n-type, possessing majority carrier electrons. The large variation in carrier concentration and carrier type is consistent with FET measurements. Samples prepared by vacuum deposition with excess Pb and Se give rise to majority carrier electrons and holes, respectively. Larger electron or hole concentrations are clearly observed when greater excess Pb or Se is deposited, respectively.

The data clearly show that carrier concentrations induced by intentional stoichiometric manipulation are much larger than unintentional or initial doping concentrations, or $\Delta n_{st} \gg n_{un} \sim n_e \sim n_h$. Quantitatively, films have $\sim 2.9 \times 10^{13}$ NCs/cm^2, assuming random packing of NCs as seen in SEM and SAXS data. Deposition of 3 Å of Pb provides $\sim 9.8 \times 10^{14}$ Pb atoms/cm^2, considering the cubic closed-packed structure of lead. Hall measurements reflect a majority carrier electron concentration of 2.2×10^{18} electrons/cm^3 or 1.5×10^{13} electrons/cm^2 in a 70 nm thick film. Therefore, on average, when 33 Pb atoms are added to one NC, 0.5 electron/NC is generated. Similarly, when 47 Se atoms are added to one NC, 0.3 hole/NC is generated. However, the actual number of Pb or Se atoms needed to generate electrons or holes is anticipated to be smaller than the number of deposited atoms due to the following reasons: (1) not all of the vacuum-deposited Pb or Se atoms are effectively bound, decreasing efficiency; (2) not all of the bound Pb or Se atoms are ionized to efficiently dope the NCs: and (3) some Pb (or Se) atoms are compensated by unintentional dopants or defect states, suppressing the electron (or hole) concentration. We note that the Hall mobility does not change dramatically when excess Pb or Se is deposited, unlike the mobility measured in the field-effect transistor geometry. This difference is attributed to filling of surface trap states in the field-effect transistor as the Fermi level shifts toward the conduction (valence) band upon application of a positive (negative) gate voltage.[39] However, there is no applied gate voltage to fill surface trap states in the Hall measurement.

We fabricate metal−semiconductor (PbSe NC film)−insulator−metal (MSIM) junctions [Figure 4A, B] to examine the carrier type, concentration, and Fermi level by capacitance−voltage (*C*−*V*) measurements using the transmission line method.[40] The total capacitance (C_{TOT}) is the sum of the capacitances in the channel (C_{CH}) and the oxide capacitance ($C_{OX,SD}$) at the source and drain electrodes, or

$$C_{TOT} = C_{CH} + C_{OX,SD} = \left(\frac{1}{C_{OX,CH}} + \frac{1}{C_{NC}}\right)^{-1} + C_{OX,SD} \quad (2)$$

where $C_{OX,SD}$ is the capacitance of the oxide in the source and drain region, $C_{OX,CH}$ is the capacitance of the oxide in the channel region, and C_{NC} is the NC thin film capacitance.[41] The equivalent circuit of the channel is shown in Figure 4B. In the accumulation region, $C_{NC} \rightarrow \infty$, and therefore $C_{CH} \rightarrow C_{OX,CH}$, so $C_{TOT} = C_{max} = C_{OX,CH} + C_{OX,SD}$.[40,42] When fully depleted, $C_{NC} \rightarrow 0$ and $C_{CH} \approx 0$, and thus $C_{TOT} = C_{min} = C_{OX,SD}$.[42]

C−*V* characteristics of as-synthesized, SCN-exchanged PbSe NC films [Figure 4 (C and D)] show p-type characteristics with a threshold voltage (V_{TH}) larger than 35 V. When Pb is deposited in increasing excess [Figure 4C], the curves show ambipolar behavior transitioning to unipolar n-type. V_{TH} shifts from positive through zero to negative voltages, which reflects the shift in the Fermi level from near the valence band to near the conduction band [Figure 1B].[41] As Pb is heavily deposited, V_{TH} shifts outside of the −35 V measurement window and the film has a high concentration of accumulated electrons with a constant capacitance of C_{max}. Complementary behavior is observed as excess Se is deposited [Figure 4D]. Initially p-type behavior in as-synthesized and exchanged PbSe NC films does not have high hole accumulation even at −35 V, and thus the capacitance is smaller than C_{max}. As more Se is deposited [Figure 4D], the capacitance increases gradually and reaches C_{max}, indicating that more holes are accumulated, consistent with the Hall and FET measurements. V_{TH} shifts toward more positive values as the Fermi level of the NC film approaches the valence band [Figure 1B]. When 1 to 2 Å of Se are deposited, V_{TH} shifts beyond the 35 V measurement window and the film has a high concentration of accumulated holes with a constant capacitance of C_{max}.

The accumulated mobile charges can be calculated by integrating the *C*−*V* characteristics according to $Q = \int_{V_{TH}}^{V} C dV$. We integrated the capacitance of as-synthesized and exchanged PbSe NC thin films from the extrapolated V_{TH} of $V_G = 50$ V to $V_G = 0$ V. The carrier concentration of the pristine NC thin film is calculated to be 6×10^{11} holes/cm^2. The carriers are accumulated within the Debye length (20 nm) of the NC film at the semiconductor−gate dielectric interface, which has 8.4×10^{12} NCs/cm^2. The carrier concentration corresponds to 0.07 hole/NC. When 0.9 Å of Pb is deposited, the film changes in behavior to n-type. Integrating the accumulated charge from the extrapolated V_{TH} of −140 V to 0 V gives 3.6×10^{12} electrons/cm^2. The excess Pb corresponds to the addition of 34 atoms/NC and an increase of 0.6 electron/NC. Similarly, when 0.3 Å of Se is deposited, integrating the accumulated charge from the extrapolated V_{TH} of 100 V to 0 V gives 3.0×10^{12} holes/cm^2. The excess Se corresponds to an addition of 16 atoms/NC and an increase of 0.15 hole/NC. The Δn_{st} found by the *C*−*V* measurements upon introduction of excess Pb and Se atoms is consistent with the values found from samples probed by Hall measurements. Each atom of excess Pb or Se, within a factor of 2, provides the same number of additional electrons and holes. This supports the interpretation that the difference in the measured current levels in Pb- and Se-rich NC FETs arises from a difference not in carrier concentration, but in carrier mobility.

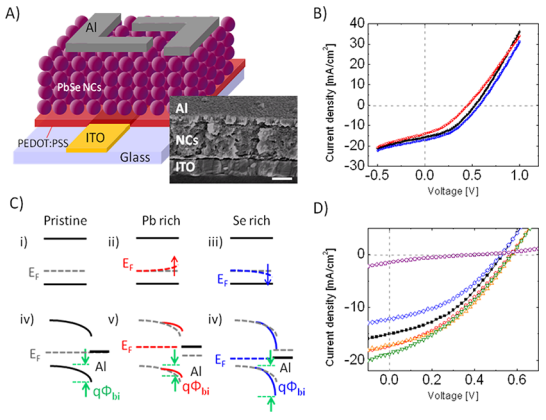

Figure 5. (A) Schematic of 2.5 nm PbSe NC Schottky solar cell and device cross sectional SEM image (scale bar: 100 nm); (B) current density−voltage characteristics of (black) pristine and after deposition of (red) 0.2 Å excess Pb and (blue) 0.2 Å excess Se; (C) band diagrams for (black) pristine, (red) Pb-rich, and (blue) Se-rich PbSe NC Schottky junctions with Al electrodes; and (D) current density−voltage characteristics of Se-rich solar cells (black) before and after (red) 0.1 Å, (orange) 0.2 Å, (green) 0.4 Å, (blue) 0.8 Å, and (purple) 2 Å of Se deposited.

We utilize nonstoichiometry to engineer the carrier concentration in PbSe NC solids integrated as the single photoactive layer in Schottky solar cells [Figure 5A].[43] PEDOT:PSS is spin-coated onto patterned ITO substrates, and the devices are annealed at 150 °C. For photovoltaics, small 2−3 nm diameter PbSe NCs with the first excitonic absorption resonance at 800−900 nm are used (optical absorption spectra in Supporting Information Figure S3 and TEM images in Supporting Information Figure S7), as larger band-gap PbSe NCs are known to provide a higher open circuit voltage.[44] Multiple layers of PbSe NCs are spin-coated and soaked in BDT in acetonitrile until the desired thickness (180 to 250 nm) is achieved. BDT is selected, as it is a strongly bound bidentate linker known to enhance photovoltaic performance.[25,44] Solar cells with active layers thicker than 250 nm show a decrease in efficiency because light absorption in the PbSe NC thin film is limited by charge generation in the depletion region formed at the PbSe NC/Al junction.[44,45] We change the stoichiometry of the films by thermally evaporating 0.2 Å of Se or 2 Å of Pb to make the surface more p-type or n-type, respectively. Aluminum electrodes are thermally evaporated through a shadow mask to complete the cell fabrication, yielding an active region of ~9 mm^2.

I−*V* curves of as-prepared, Pb-rich, and Se-rich PbSe NC Schottky cells are shown in Figure 5B. While excess Pb reduces the open circuit voltage (V_{OC}) and efficiency, excess Se increases the V_{OC} and efficiency. Schematic band diagrams of as-prepared, Pb-rich, and Se-rich NC solids are shown in Figure 5C. As the NC surface becomes n-type (p-type) due to the deposition of excess Pb (Se), the Fermi level moves closer to the conduction (valence) band. When the semiconductor−metal contact is formed, band bending

occurs to align the Fermi level between the metal and semiconductor.[46] While excess Pb reduces the band-bending at the interface, the more strongly p-type interface with excess Se desirably increases band-bending. We note that while the Fermi level moves closer to the conduction (valence) band with excess Pb (Se), the electron (hole) mobility in the solar cell is more appropriately represented by Hall measurements than by FET measurements. In solar cells low-level injection does not shift the quasi-Fermi level sufficiently toward the conduction (valence) band to fill trap states within the energy gap.

We vary the excess Se from 0 to 2 Å to manipulate the band-bending at the metal−semiconductor interface in NC Schottky solar cells [Figure 5D]. Initially as the amount of Se is increased, the V_{OC} and efficiency increase, but after some critical point the efficiency begins to decrease. The decrease in solar cell efficiency at higher levels of excess Se may arise from (1) heavily degenerate doping of the interface[47] and/or (2) reduced carrier lifetime due to increased impurities.[48] Maximum power conversion efficiencies of up to 3.85% are realized by introducing 0.2 Å of excess Se, enhanced in comparison to efficiencies of 3.5% in reference as-prepared NC thin film devices.

CONCLUSIONS

In summary, we show that the carrier statistics in lead chalcogenide NC thin films can be precisely controlled by stoichiometric imbalance. We have studied the relationship between excess Pb and Se and the carrier type, concentration, and Fermi level in lead chalcogenide NC thin film solids. We applied this method to build robust and high-performance unipolar n- and p-type NC field effect transistors at room temperature as well as solar cells with increased power conversion efficiency. This study contributes to the fundamental understanding of the electronic properties of lead chalcogenide nanostructures and the role of stoichiometric imbalance in engineering this family of materials for various applications such as thermoelectrics, electronics, and optoelectronics.

METHODS

Materials. Tri-*n*-octylphosphine (further referred to as TOP, 90%), oleic acid (OA, 90%), 1-octadecene (ODE, 90%), lead oxide (PbO, 99.999%), selenium pellets (Se, 99.999%), diphenylphosphine (DPP, 98%), (3-mercaptopropyl)trimethoxysilane (MPTS, 95%), ammonium thiocyanate (99+%), hydrazine (98%), 1,2-ethanedithiol (EDT, ≥98%), 1,3-benzenedithiol (BDT, >98%), anhydrous chloroform, anhydrous hexane, anhydrous 2-propanol, anhydrous methanol, anhydrous toluene, and anhydrous acetonitrile were purchased from Aldrich. Anhydrous acetone and bis(trimethylsilyl) sulfide (TMS, 95%) were purchased from Acros. *n*-Octadecylphosphonic acid (ODPA, PCI synthesis, 99%) was purchased from PCI synthesis. Bis(trimethylsilyl) selenide ($(TMS)_2Se$) was bought from Gelest. Lead (Pb, 99.999% purity) and selenium (Se, 99.999%) for thermal evaporation were purchased from Kurt J. Lesker. Ethanol was dried using standard procedures.

Synthesis of PbSe NCs. *6 nm PbSe NCs.* Synthesis of 6 nm PbSe nanocrystals was performed using a slight modification of a previously reported procedure.[49] Nanocrystal synthesis was carried out under a nitrogen atmosphere with a Schlenk line system using standard air-free procedures. A solution of 892 mg of PbO, 3 mL of oleic acid, and 20 mL of ODE was heated to 120 °C and degassed for 1 h under vacuum. The temperature was then raised to 180 °C, at which 8 mL of the Se precursor (1 M TOP:Se and 60 μL of DPP) was rapidly injected into the hot solution. After 80 s of reaction time, the solution was rapidly cooled to room temperature using an ice bath. The nanocrystals were purified within a nitrogen glovebox by first adding 2 mL of hexane to the reaction flask, then precipitating the solution with ethanol/2-propanol, centrifuging at 8000 rpm for 3 min, and redisperseing in 4 mL of hexane. The wash process was repeated three more times using ethanol, acetone/2-propanol, and then 2-propanol as the antisolvents. Finally, the nanocrystals were dispersed in 5 mL of hexane and stored in the glovebox. Before the nanocrystals were deposited, the solution was dried under vacuum to remove the hexane, and the NCs were redispersed in octane.

2−3 nm PbSe NCs. Synthesis of 2−3 nm PbSe nanocrystals was performed using a slight modification of the previously reported procedure.[44] A solution of 446 mg of PbO, 1.55 mL of oleic acid, and 25 mL of ODE was heated to 180 °C and degassed at 120 °C for 1 h under vacuum. The temperature was then increased to 140 °C, after which 124 μL of a Se precursor, $(TMS)_2Se$ in 8 mL ODE (***NOTE: Bis(trimethylsilyl) selenide is toxic by vapor inhalation and skin absorption***), was injected into the hot solution quickly. After 100 s of reaction, the solution was rapidly cooled to room temperature using an ice bath. The nanocrystals were purified by precipitation twice in hexane/2-propanol, once in hexane/ethanol, and once in hexane/acetone, after which they were stored in hexane in a nitrogen glovebox.

Synthesis of PbS NCs. *5 nm PbS NCs.* The synthesis of 5 nm PbS nanocrystals was performed using a previously reported method.[50] A 470 mg amount of PbO and 15 mL of oleic acid were heated in a 50 mL flask to 120 °C and degassed under vacuum on a Schlenk line for 2 h. During this time, a 42 μL TMS/2 mL ODE solution was prepared in a nitrogen glovebox. After degassing, the reaction solution was put under nitrogen and the temperature lowered to 110 °C, at which point 5 mL of the TMS/ODE sulfur precursor solution was rapidly injected. After a growth time of 50 s, the reaction solution was quenched in a water bath. The NCs were then washed by adding 5 mL of hexane to the solution, then precipitating with 10 mL of ethanol, centrifuging at 8000 rpm for 3 min, and decanting the supernatant. NCs were washed a second and third time by redispersing the pellet in 6 mL of hexane, precipitating with 6 mL of ethanol, and centrifuging at 8000 rpm for 3 min. NCs were then redispersed in 10 mL of hexane and stored in a nitrogen glovebox. Before the nanocrystals were deposited, the solution was dried under vacuum to remove the hexane, and the NCs were redispersed in octane.

Ligand Exchange. All the ligand exchanges were conducted under a nitrogen atmosphere. The original ligands derivatizing the NCs were exchanged for shorter ligands by various methods. For the SCN exchange, spin-coated PbSe NC films were dipped in methanol for 1 min to wash off excess ligand, then in SCN (1% vol in MeOH) for 1 min, and finally washed with methanol again to remove excess SCN. For the EDT exchange, the NC films were dipped in 0.1 M EDT in acetonitrile for 5 min and washed with toluene. For BDT, the NC films were dipped in 0.1 M BDT in acetonitrile and washed with toluene. Finally, for the hydrazine treatment, the NC films were dipped in 1 M hydrazine (***NOTE: hydrazine is toxic by vapor inhalation and skin absorption***) for 5 min and washed with acetonitrile.

Device Fabrication. All the fabrications were conducted under a nitrogen atmosphere after substrate cleaning and treatment with a self-assembled monolayer, unless specified.

Devices for FET and CV measurements were fabricated on heavily n-doped silicon wafers with 250 nm of thermally grown SiO_2, which serve as the back gate and part of the gate dielectric stack, respectively. The substrate was washed with DI water, acetone, and IPA and cleaned with UV-ozone for 30 min. A 20 nm layer of Al_2O_3 was deposited by atomic layer deposition on top of the SiO_2, after which the substrate was cleaned with chloroform and acetone before being subjected to 30 more minutes of UV-ozone to ensure that there was no buildup of unwanted organics. The substrate was then immersed in octadecylphosphonic acid in IPA for 16 h to create an organic monolayer of ODPA. When the substrate was removed from the solution, it was rinsed with clean IPA and heated to 70 °C for 10 min. To make the devices, the substrates were first cleaned again with chloroform and acetone and then transferred to the nitrogen glovebox. A solution of 10 mg/mL PbSe NCs in octane was spin-coated at 800−1200 rpm to deposit a uniform nanocrystal thin film solid, and the original oleic acid ligands were replaced with various shorter ligands, using the ligand exchange processes described above. The 40 nm Au source and drain top contacts separated by 50−150 μm were defined by thermal evaporation through a shadow mask. Channel lengths (L) and widths (W) were a constant W/L of 15 for all devices. Finally, individual devices were carefully mechanically isolated both from each other and from the edges of the substrate to minimize leakage current.

Devices for the Hall measurements were fabricated on quartz. The substrate was cleaned with DI water, acetone, and IPA and cleaned with UV-ozone for 30 min. Then the substrate was immersed in 5% MPTS in toluene for 16 h. A solution of 20 mg/mL PbSe NCs in octane was spin-coated onto the substrate, and the oleic acid ligand was exchanged with SCN. The spin-coating and ligand exchange procedures were repeated until the desired film thickness of 70 nm was achieved. Four square Au electrodes (1 mm^2) separated from each other by 5 mm in a square pattern were defined by thermal evaporation through a shadow mask. Each device was isolated by carefully scraping away the film around the square defined by the electrodes with a toothpick.

Fabrication of PbSe NC Schottky solar cells was performed using a slight modification of the previously reported procedure.[43] Photovoltaic cells were fabricated on patterned ITO on glass substrates. A film of PEDOT:PSS (3−40 nm, Clevios) was spin-coated on the substrate and dried at 150 °C for 15 min in air. A solution of 40 mg/mL PbSe NCs in octane/hexane (4:1) was spin-coated on top of the PEDOT:PSS film in a nitrogen glovebox. Devices were soaked in 1 mM BDT in acetonitrile for a few minutes and washed with toluene to exchange the ligands. Multiple layers of PbSe NCs were spin-coated until the desired thickness was achieved. Aluminum electrodes were thermally evaporated through a shadow mask.

Excess Pb or Se Deposition. Using an evaporator integrated into our nitrogen glovebox, Pb and Se were deposited onto the NC thin film samples, with a source-to-sample distance of 30 cm, by thermal evaporation at a base pressure of 8×10^{-7} Torr at an evaporation rate between 0.01 and 0.03 Å/s.

Measurement and Characterization. All the measurements were conducted in an inert glovebox atmosphere unless otherwise specified. FET characterization was performed on a model 4156C semiconductor parameter analyzer (Agilent) in combination with a Karl Suss PM5 probe station mounted in a nitrogen glovebox.

Capacitance−voltage characterization was conducted on a model 4192A LF impedance analyzer (Agilent) in a nitrogen glovebox. Source and drain electrodes were electrically shorted and connected to the low terminal and the gate was connected to the high terminal of the LCR meter. $C-V$ curves were measured in the range 100 to 5 kHz, and the representative data were obtained at 500 Hz.

The Hall measurements were carried out using an MMR Technologies H-50 measurement system with a 0.5 T magnet inside a nitrogen glovebox. Each measurement was preceded by a four-point probe resistivity measurement using the Van der Pauw geometry.

Current−voltage data on solar cell geometry samples were obtained using a Keithley 2400 source-meter under the illumination of AM 1.5G solar simulated light (1 sun, 100 mW/cm^2, Oriel instruments model 96000, Newport Co.) in the sealed cell with a nitrogen atmosphere. The light intensity was calibrated with a reference cell and meter (model 91150, Newport Co.).

X-ray Diffraction. PbSe nanocrystal thin films were spin-cast on quartz substrates. Wide-angle X-ray diffraction measurement was carried out with a Rigaku Smartlab high-resolution diffractometer using Cu Kα radiation. Small-angle X-ray scattering patterns were performed on a multiangle X-ray diffractometer using a Bruker HiStar Multiwire 2-D area detector and a Bruker FR591 copper rotating anode operated at 40 kV and 85 mA (Cu Kα radiation). Small-angle X-ray scattering data were analyzed using Datasqueeze software.

Conflict of Interest: The authors declare no competing financial interest.

Acknowledgment. The synthesis of PbS and PbSe nanocrystals and the fabrication and characterization of bottom-contact field-effect transistors used to study the diffusion length of lead and selenium, devices for Hall-effect measurements, and Schottky barrier solar cells were supported by the U.S. Department of Energy Office of Basic Energy Sciences, Division of Materials Science and Engineering, under Award No. DE-SC0002158. Optical absorption spectra and the fabrication of top-contact field-effect transistors and their characterization as transistors and in capacitance−voltage measurements as a function of stoichiometric imbalance was supported by the NSF MRSEC Program under Award No. DMR05-1120901. Small- and wide-angle X-ray diffraction and scanning electron microscopy was supported by the Office of Naval Research Multidisciplinary University Research Initiative Award No. ONR-N00014-10-1-0942. Scanning electron microscopy was performed in facilities supported by NSF MRSEC Program under Award No. DMR05-1120901.

Supporting Information Available: Experimental details and supplementary figures as described in the text. This material is available free of charge *via* the Internet at http://pubs.acs.org.

REFERENCES AND NOTES

1. Talapin, D. V.; Murray, C. B. PbSe Nanocrystal Solids for n- and p-Channel Thin Film Field-Effect Transistors. *Science* **2005**, *310*, 86–89.
2. Koh, W.; Saudari, S. R.; Fafarman, A. T.; Kagan, C. R.; Murray, C. B. Thiocyanate-Capped PbS Nanocubes: Ambipolar Transport Enables Quantum Dot-Based Circuits on a Flexible Substrate. *Nano Lett.* **2011**, *11*, 4764–4767.
3. Wang, R. Y.; Feser, J. P.; Lee, J.-S.; Talapin, D. V.; Segalman, R.; Majumdar, A. Enhanced Thermopower in PbSe Nanocrystal Quantum Dot Superlattices. *Nano Lett.* **2008**, *8*, 2283–2288.
4. Ip, A. H.; Thon, S. M.; Hoogland, S.; Voznyy, O.; Zhitomirsky, D.; Debnath, R.; Levina, L.; Rollny, L. R.; Carey, G. H.; Fischer, A.; *et al.* Hybrid Passivated Colloidal Quantum Dot Solids. *Nat. Nanotechnol.* **2012**, *7*, 577–582.
5. Sukhovatkin, V.; Hinds, S.; Brzozowski, L.; Sargent, E. H. Colloidal Quantum-Dot Photodetectors Exploiting Multiexciton Generation. *Science* **2009**, *324*, 1542–1544.
6. Semonin, O. E.; Luther, J. M.; Choi, S.; Chen, H.-Y.; Gao, J.; Nozik, A. J.; Beard, M. C. Peak External Photocurrent Quantum Efficiency Exceeding 100% *via* MEG in a Quantum Dot Solar Cell. *Science* **2011**, *334*, 1530–1533.
7. Tang, J.; Kemp, K. W.; Hoogland, S.; Jeong, K. S.; Liu, H.; Levina, L.; Furukawa, M.; Wang, X.; Debnath, R.; Cha, D.; *et al.* Colloidal-Quantum-Dot Photovoltaics Using Atomic-Ligand Passivation. *Nat. Mater.* **2011**, *10*, 765–771.
8. Efros, A. L.; Efros, A. L. Interband Absorption of Light in a Semiconductor Sphere. *Sov. Phys. Semicond.* **1982**, *16*, 772–775.
9. Luther, J. M.; Law, M.; Song, Q.; Perkins, C. L.; Beard, M. C.; Nozik, A. J. Structural, Optical, and Electrical Properties of Self-Assembled Films of PbSe Nanocrystals Treated with 1,2-Ethanedithiol. *ACS Nano* **2008**, *2*, 271–280.

10. Leschkies, K. S.; Kang, M. S.; Aydil, E. S.; Norris, D. J. Influence of Atmospheric Gases on the Electrical Properties of PbSe Quantum-Dot Films. *J. Phys. Chem. C* **2010**, *525*, 9988–9996.
11. Ravich, U. I. *Semiconducting Lead Chalcogenides*; Plenum Press: New York, 1970.
12. Allgaier, R. S.; Scanlon, W. W. Mobility of Electrons and Holes in PbS, PbSe, and PbTe between Room Temperature and 4.2 K. *Phys. Rev.* **1958**, *111*, 1029–1037.
13. Schlichting, U.; Gobrecht, K. The Mobility of Free Carriers in PbSe Crystals. *J. Phys. Chem. Solids* **1973**, *34*, 753–758.
14. Logothetis, E.; Holloway, H. Compensation and Ionized Defect Scattering in PbTe. *Solid State Commun.* **1970**, *8*, 1937–1940.
15. Moreels, I.; Lambert, K.; Muynck, D. D. Composition and Size-Dependent Extinction Coefficient of Colloidal PbSe Quantum Dots. *Chem. Mater.* **2007**, *19*, 6101–6106.
16. Moreels, I.; Fritzinger, B.; Martins, J. C.; Hens, Z. Surface Chemistry of Colloidal PbSe Nanocrystals. *J. Am. Chem. Soc.* **2008**, *130*, 15081–15086.
17. Fafarman, A. T.; Koh, W.-K.; Diroll, B. T.; Kim, D. K.; Ko, D.-K.; Oh, S. J.; Ye, X.; Doan-Nguyen, V.; Crump, M. R; Reifsnyder, D. C.; *et al*. Thiocyanate Capped Nanocrystal Colloids: A Vibrational Reporter of Surface Chemistry and a Solution-Based Route to Enhanced Coupling in Nanocrystal Solids. *J. Am. Chem. Soc.* **2011**, *133*, 15753–15761.
18. Choi, J.-H.; Fafarman, A. T.; Oh, S. J.; Ko, D.-K.; Kim, D. K.; Diroll, B. T.; Muramoto, S.; Gillen, J. G.; Murray, C. B.; Kagan, C. R. Bandlike Transport in Strongly Coupled and Doped Quantum Dot Solids: A Route to High-Performance Thin-Film Electronics. *Nano Lett.* **2012**, *12*, 2631–2638.
19. Liu, Y.; Gibbs, M.; Puthussery, J.; Gaik, S.; Ihly, R.; Hillhouse, H. W.; Law, M. Dependence of Carrier Mobility on Nanocrystal Size and Ligand Length in PbSe Nanocrystal Solids. *Nano Lett.* **2010**, *10*, 1960–1969.
20. Talgorn, E.; Gao, Y.; Aerts, M.; Kunneman, L. T.; Schins, J. M.; Savenije, T. J.; van Huis, M.; van der Zant, H. S. J.; Houtepen, A. J.; Siebbeles, L. D. Unity Quantum Yield of Photogenerated Charges and Band-Like Transport in Quantum-Dot Solids. *Nat. Nanotechnol.* **2011**, *6*, 733–739.
21. Law, M.; Beard, M. C.; Choi, S.; Luther, J. M.; Hanna, M. C.; Nozik, A. J. Determining the Internal Quantum Efficiency of PbSe Nanocrystal Solar Cells with the Aid of an Optical Model. *Nano Lett.* **2008**, *8*, 3904–3910.
22. Beard, M. C.; Midgett, A. G.; Law, M.; Semonin, O. E.; Ellingson, R. J.; Nozik, A. J. Variations in the Quantum Efficiency of Multiple Exciton Generation for a Series of Chemically Treated PbSe Nanocrystal Films. *Nano Lett.* **2009**, *9*, 836–845.
23. Kang, M.; Lee, J.; Norris, D.; Frisbie, C. High Carrier Densities Achieved at Low Voltages in Ambipolar PbSe Nanocrystal Thin-Film Transistors. *Nano Lett.* **2009**, *9*, 3848–3852.
24. Law, M.; Luther, J. M.; Song, Q.; Hughes, B. K.; Perkins, C. L.; Nozik, A. J. Structural, Optical, and Electrical Properties of PbSe Nanocrystal Solids Treated Thermally or with Simple Amines. *J. Am. Chem. Soc.* **2008**, *130*, 5974–5985.
25. Koleilat, G.; Levina, L.; Shukla, H.; Myrskog, S. Efficient, Stable Infrared Photovoltaics Based on Solution-Cast Colloidal Quantum Dots. *ACS Nano* **2008**, *2*, 833–840.
26. Liu, Y.; Gibbs, M.; Perkins, C. L.; Tolentino, J.; Zarghami, M. H.; Bustamante, J.; Law, M. Robust, Functional Nanocrystal Solids by Infilling with Atomic Layer Deposition. *Nano Lett.* **2011**, *11*, 5349–5355.
27. Koole, R.; Liljeroth, P. Electronic Coupling and Exciton Energy Transfer in CdTe Quantum-Dot Molecules. *J. Am. Chem. Soc.* **2006**, *128*, 10436–10441.
28. Oh, S. J.; Kim, D. K.; Kagan, C. R. Remote Doping and Schottky Barrier Formation in Strongly Quantum Confined Single PbSe Nanowire. *ACS Nano* **2012**, *6*, 4328–4334.
29. Kim, D. K.; Lai, Y. L.; Vemulkar, T. R.; Kagan, C. R. Flexible, Low Voltage, and Low Hysteresis PbSe Nanowire Field Effect Transistors. *ACS Nano* **2011**, *5*, 10074–10083.
30. Petkov, V.; Moreels, I.; Hens, Z.; Ren, Y. PbSe Quantum Dots: Finite, Off-Stoichiometric, and Structurally Distorted. *Phys. Rev. B* **2010**, *81*, 241304(1−4).
31. Kim, D. K.; Vemulkar, T. R.; Oh, S. J.; Koh, W.-K.; Murray, C. B.; Kagan, C. R. Ambipolar and Unipolar PbSe Nanowire Field-Effect Transistors. *ACS Nano* **2011**, *5*, 3230–3236.
32. Moon, S.; Lee, S.-G.; Song, W.; Lee, J. S.; Kim, N.; Kim, J.; Park, N. Fabrication of n-Type Nanotube Transistors with Large-Work-Function Electrodes. *Appl. Phys. Lett.* **2007**, *90*, 092113(1−3).
33. Kang, M. S.; Sahu, A.; Norris, D. J.; Frisbie, C. D. Size- and Temperature-Dependent Charge Transport in PbSe Nanocrystal Thin Films. *Nano Lett.* **2011**, *11*, 3887–3892.
34. Gai, Y.; Peng, H.; Li, J. Electronic Properties of Nonstoichiometric PbSe Quantum Dots from First Principles. *J. Phys. Chem. C* **2009**, *113*, 21506–21511.
35. While all other FET measurements were conducted in top contact configuration, as top contact structures form higher mobility devices, diffusion length studies as a function of film thickness were carried out using bottom contact structures. When the film is thick in top contact devices, resistance between the electrode and the channel, known as "access resistance", increases. This phenomenon can be avoided in the case of bottom contact devices, as the metal electrode is in direct contact with the NC thin film channel.
36. Tang, J.; Liu, H.; Zhitomirsky, D.; Hoogland, S.; Wang, X.; Furukawa, M.; Levina, L.; Sargent, E. H. Quantum Junction Solar Cells. *Nano Lett.* **2012**, *12*, 4889–4894.
37. Zhitomirsky, D.; Furukawa, M.; Tang, J.; Stadler, P.; Hoogland, S.; Voznyy, O.; Liu, H.; Sargent, E. H. N-Type Colloidal Quantum Dot Solids for Photovoltaics. *Adv. Mater.* **2012**, *24*, 6181–6185.
38. Ning, Z.; Ren, Y.; Hoogland, S.; Voznyy, O.; Levina, L.; Stadler, P.; Lan, X.; Zhitomirsky, D.; Sargent, E. H. All-Inorganic Colloidal Quantum Dot Photovoltaics Employing Solution-Phase Halide Passivation. *Adv. Mater.* **2012**, *24*, 6295–6299.
39. Shur, M.; Hack, M. Physics of Amorphous Silicon Based Alloy Field-Effect Transistors. *J. Appl. Phys.* **1984**, *55*, 3831–3842.
40. Greve, D. W.; Hay, V. R. Interpretation of Capacitance-Voltage Characteristics of Polycrystalline Silicon Thin-Film Transistors. *J. Appl. Phys.* **1987**, *61*, 1176–1180.
41. Sze, S. M.; Ng, K. K. *Physics of Semiconductor Devices*, 3rd ed.; John Wiley & Sons: Hoboken, NJ, 2007.
42. Hamadani, B. H.; Richter, C. A.; Suehle, J. S.; Gundlach, D. J. Insights into the Characterization of Polymer-Based Organic Thin-Film Transistors Using Capacitance-Voltage Analysis. *Appl. Phys. Lett.* **2008**, *92*, 203303(1−3).
43. Luther, J. M.; Law, M.; Beard, M. C.; Song, Q.; Reese, M. O.; Ellingson, R. J.; Nozik, A. J. Schottky Solar Cells Based on Colloidal Nanocrystal Films. *Nano Lett.* **2008**, *8*, 3488–3492.
44. Ma, W.; Swisher, S.; Ewers, T.; Engel, J.; Ferry, V. E.; Atwater, H. A.; Alivisatos, A. P. Photovoltaic Performance of Ultra-Small PbSe Quantum Dots. *ACS Nano* **2011**, *5*, 8140–8147.
45. Pattantyus-Abraham, A.; Kramer, I. Depleted-Heterojunction Colloidal Quantum Dot Solar Cells. *ACS Nano* **2010**, *4*, 3374–3380.
46. Rhoderick, E. H. *Metal-Semiconductor Contacts*, 2nd ed.; Claredon Press: Oxford, 1988.
47. Nelsons, J. *The Physics of Solar Cells*; Imperial College Press: London, 2003.
48. Zogg, H.; Vogt, W.; Baumgartner, W. Carrier Recombination in Single Crystal PbSe. *Solid-State Electron. Solid-State Electron.* **1982**, *25*, 1147–1155.
49. Yu, W. W.; Falkner, J. C.; Shih, B. S.; Colvin, V. L. Preparation and Characterization of Monodisperse PbSe Semiconductor Nanocrystals in a Noncoordinating Solvent. *Chem. Mater.* **2004**, *35*, 3318–3322.
50. Hines, M. a.; Scholes, G. D. Colloidal PbS Nanocrystals with Size-Tunable Near-Infrared Emission: Observation of Post-Synthesis Self-Narrowing of the Particle Size Distribution. *Adv. Mater.* **2003**, *15*, 1844–1849.